



# Combination of chemical foaming and direct ink writing for lightweight geopolymers

Camille Zoude, Laurent Gremillard, Elodie Prud'Homme

## ► To cite this version:

Camille Zoude, Laurent Gremillard, Elodie Prud'Homme. Combination of chemical foaming and direct ink writing for lightweight geopolymers. Open Ceramics, 2023, 16, pp.100478. <10.1016/j.oceram.2023.100478>. <hal-04229174>

**HAL Id: hal-04229174**

**<https://hal.science/hal-04229174v1>**

Submitted on 5 Oct 2023

**HAL** is a multi-disciplinary open access archive for the deposit and dissemination of scientific research documents, whether they are published or not. The documents may come from teaching and research institutions in France or abroad, or from public or private research centers.

L'archive ouverte pluridisciplinaire **HAL**, est destinée au dépôt et à la diffusion de documents scientifiques de niveau recherche, publiés ou non, émanant des établissements d'enseignement et de recherche français ou étrangers, des laboratoires publics ou privés.



Distributed under a Creative Commons CC BY-NC-ND 4.0 - Attribution - Non-commercial use - No Derivative Works - International License



# Combination of chemical foaming and direct ink writing for lightweight geopolymers

Camille Zoude<sup>\*</sup>, Laurent Gremillard, Elodie Prud'Homme

Univ Lyon, INSA Lyon, Université Claude Bernard Lyon 1, CNRS, MATEIS, UMR5510, 69621, Villeurbanne, France

## ARTICLE INFO

### Keywords:

3D printing  
Porous geopolymer  
Organic additives

## ABSTRACT

In this work, the possibility of combining direct ink writing and chemical foaming to create geopolymer lattices with interconnecting porosity at different scales is investigated. Chemical foaming was achieved by introducing aluminum powder into the paste, in order to produce a foam which was then 3D printed. Homogeneous foams with interconnected pores were generated, by combining polyethylene glycol, hexadecyltrimethylammonium bromide and aluminum powder. Porosity was characterized by X-ray tomography, mercury intrusion porosimetry and helium pycnometry. The samples obtained after the 3D printing of the foams have a similar open porosity than foams directly molded. However, their pore access diameters are very different since the 3D printing process tends to close the channels generated by the gas escape during chemical foaming. This loss is compensated by the porosity created by 3D printing, which is due to the space between the filaments.

## 1. Introduction

Porous geopolymers are promising materials for many applications such as heavy metals or synthetic dyes adsorption, thermal and sound insulation, catalyst support, evaporative cooling, pH value regulators or energy storage [1–5]. The materials developed here will find application in the field of thermochemical energy storage which requires a higher open porosity, with interconnection at different scales from the macroscopic level to the nanoscopic level.

To synthesize a geopolymer, a solid aluminosilicate generally reacts with a highly concentrated aqueous alkali hydroxide or silicate solution to form a synthetic alkali aluminosilicate material [6]. These materials usually present an open porosity up to 40% with pore sizes ranging from a few ångström to the millimeter, depending on initial composition and processing parameters [7]. But the application of thermochemical energy storage requires higher and more connected porosity at different scales [8]. There are several methods to increase the porosity within geopolymers which are the subject of numerous reviews [9–11].

One of them consists in adding sacrificial components (like polymers, water in the ice templating method [12] or organic oil in the emulsion templating [13]) to the geopolymer slurry. The porosity is then generated by dissolution, melting or thermal decomposition of the components.

The most common method is the direct foaming method which

includes mechanical foaming and chemical foaming. In mechanical foaming, a premade foam is blended with the geopolymer paste or surfactants are added to the mixture to trapped bubbles during the mixing process by air entrainment. In chemical foaming, a blowing agent is added (e.g. hydrogen peroxide, fine metallic powders) into the geopolymer paste [14]. In reaction with the alkaline environment, gas is generated and trapped within the slurry.

More recently, additive manufacturing (AM) and particularly Direct Ink Writing (DIW) has successfully been applied to geopolymers to fabricate a wide range of porous components [15–17]. The geopolymer slurry, whose rheology is adapted to the printing process, is extruded in the form of filaments through a nozzle whose position is controlled in the three dimensions of space. The filaments are assembled layer by layer to form a more or less complex part. This total control of the structure, and in particular of the space between the filaments, allows to tailor the size of the pores, their distribution, their shape and their connectivity.

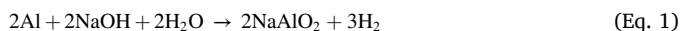
Some studies report the combination of these methods in order to create hierarchically porous geopolymer. For example, B. Coppola et al. used direct ink writing to print alkali-activated pastes containing polymethyl methacrylate (PMMA) beads as sacrificial fillers [18]. S. Yan et al. combined hydrogen peroxide (chemical foaming agent) with dolomite hollow microspheres [19]. But, to our knowledge, no paper reports the combination of chemical foaming and direct ink writing in

<sup>\*</sup> Corresponding author.

E-mail address: [camille.zoude@insa-lyon.fr](mailto:camille.zoude@insa-lyon.fr) (C. Zoude).

the case of geopolymers.

In this work, porous geopolymers were obtained using two methods: direct ink writing and chemical foaming. These two techniques were first applied independently of each other in order to study the porosity of the structures obtained. The chemical foaming agent chosen is aluminum powder. The reaction leading to the release of dihydrogen is as follows [9]:



The impact of different organic additives (one rheological modifier and two surfactants) and of the concentration of aluminum powder was studied in the case of chemical foaming. These two techniques were then combined in order to create hierarchically porous geopolymers with pores both between the filaments (obtained by direct ink writing) and in the filaments themselves (obtained by chemical foaming). Particular attention has been paid to the impact of direct ink writing on porosity.

## 2. Materials and methods

### 2.1. Raw materials

Metakaolin ARGICAL-M 1000, provided by Imerys, was used as aluminosilicate source. The activation solution was a mixture of a commercial sodium silicate solution (molar ratio: Si/Na = 1.1, density:  $1.5 \text{ g cm}^{-3}$ , 60 wt% water) and sodium hydroxide pellets (97% purity), both obtained from Fisher Scientific, UK.

To induce a shear thinning behavior necessary for printing, polyethylene glycol (PEG) with an average molecular weight of  $1500 \text{ g mol}^{-1}$  (PROLABO) was used.

To generate foams, metallic aluminum powder (Thermo Fisher, 99.5% purity, particle size less than  $45 \mu\text{m}$ ), referred to as Al, was introduced as a foaming agent.

Finally, in order to stabilize these foams, the effect of two surfactants was studied: hexadecyltrimethylammonium bromide (CTAB, Sigma-Aldrich) and sodium dodecyl sulfate (SDS, Sigma-Aldrich).

### 2.2. Paste preparation

The activation solution was prepared first. Sodium hydroxide pellets and, depending on the composition, polyethylene glycol flakes, were dissolved into sodium silicate solution. The solution was mixed until its return to room temperature after complete dissolution of the solids. It was then homogenized in a planetary mixer (SpeedMixer, Synergy devices limited) for 30 s at 800 rpm.

Metakaolin and the possible surfactants were gradually added and mixed manually for 30 s before being placed for 1 min in the planetary mixer at 800 rpm.

For mixtures containing aluminum powder, this duration was reduced to 30 s because the mixture will undergo a final mixing step, during which the aluminum powder is added. The paste is again mixed in the planetary mixer for 30 s.

Rheology of the pastes was evaluated visually at each step of their preparation to assess their homogeneity and overall rheological behavior.

All the geopolymers in this study present the following molar ratios:  $\text{SiO}_2/\text{Al}_2\text{O}_3 = 3.73$ ,  $\text{Na}_2\text{O}/\text{Al}_2\text{O}_3 = 0.95$ ,  $\text{H}_2\text{O}/\text{Na}_2\text{O} = 10.5$ .

### 2.3. Samples preparation

The final mixture was poured into  $16 \times 16 \times 20 \text{ mm}^3$  rectangular molds or 5 mL syringes (Nordson EFD, USA).

When the mixture contained aluminum powder, the samples were left in the open air for 20 min to allow the foam to form, the excess foam was removed and the containers were sealed. When the mixture did not contain aluminum powder, the containers were directly sealed.

All the samples were left for 1 h at room temperature.

After that time, mixtures in syringes were shaped by direct ink writing using a Robocasting device (3D-Inks, Tulsa, OK, USA), with tips of  $840 \mu\text{m}$  inner diameter (Nordson EFD, USA) at room temperature. An interpenetration of 15% of the tip diameter between two layers ensured the cohesion between successive layers. Parts were all printed as porous lattice of dimension  $13.7 \times 13.7 \times 11.8 \text{ mm}^3$  with  $90^\circ$  disorientation between successive layers. Filament were deposited on a printing substrate made of a flat glass plate covered with a smooth polymer sheet (copier polyester transparency film).

Once the printing is finished, all the samples (printed or molded) are subjected to a 3-step drying process described by Fig. 1.

Finally, the samples spent one night at  $100^\circ\text{C}$ , in order to remove all the water, before being characterized.

### 2.4. Samples designation

For simplification purposes, the following nomenclature will be applied to the geopolymers (G) studied in this article:

GPC/S xAl M/R

Whose terms designate the following:

- P: presence of 4.5 wt% polyethylene glycol (with respect to the total mass excluding organic additives and aluminum).
- C/S: nature of the surfactant, CTAB (C) is present at 0.5 wt%, SDS (S) at 2 wt% (with respect to the total mass excluding organic additives and aluminum).
- xAl: amount of aluminum powder, can be 0, 0.1, 0.2, 0.5 or 1 wt% of metakaolin.
- M/R: geopolymer shaping, can be molded (M) or robocast (R).

For example, the designation GPC 0.5Al R refers to a geopolymer shaped by robocasting (a lattice) containing 4.5 wt% polyethylene glycol, 0.5 wt% CTAB and 0.5 wt% aluminum powder. If a letter is absent (P, C or S), the composition does not contain the corresponding additive.

### 2.5. Samples characterization

Different types of densities were measured to characterize the porosities of the samples.

The true density ( $\rho_T$ ), corresponding to the ratio of the mass of the dry matter of the sample to its volume excluding any type of pores (closed or open), was measured using a helium pycnometer (Micromeritics AccuPyc II 1340) on 3 geopolymer powders of each composition on 100 measurement cycles.

The skeletal density ( $\rho_S$ ) was determined using mercury intrusion porosimetry (Autopore V, Micromeritics, GA, USA). This density corresponds to the ratio of the mass of the dry matter to the volume including

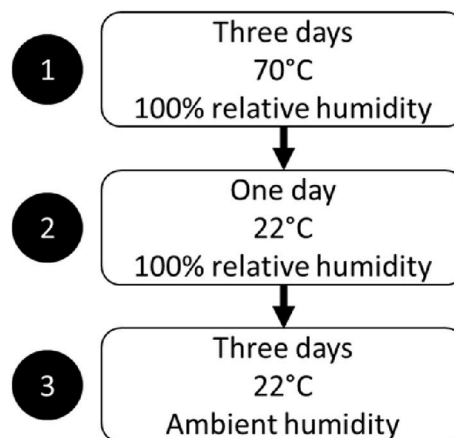


Fig. 1. Protocol for curing geopolymer samples.

only closed pores. Mercury intrusion porosimetry also enables to quantify the pore access diameter distribution, for pore access diameters between 4 nm and 300  $\mu\text{m}$ . The results were corrected with the built-in blank correction formula. Three geopolymers of each composition were tested and two types of graphs were plotted. The first represents the cumulative pore volume as a function of the pore access diameter. The minimum, maximum curve and the mean of the three curves were plotted for each composition to evidence the distribution of the data. The second represents the pore access diameter as a function of the log differential intrusion; only the median curve was plotted.

The envelop density ( $\rho_e$ ) was obtained by measuring the weight and outer volume of at least 5 samples.

For the lattices, the porosity between the filaments (IFP, for inter filament porosity), of access diameter too large to be detected by mercury intrusion, was determined by X-ray tomography using an isotropic voxel size of 7  $\mu\text{m}$ . The results were obtained on 300 images and the uncertainty was calculated by averaging the results from a thresholding considered to be correct, a thresholding considered to be slightly overestimated and a thresholding considered to be slightly underestimated. The raw data were analysed using Fiji software.

The total (TP) and open porosity (OP) relative to the total volume were calculated according to the following equations:

$$TP = \left(1 - \frac{\rho_e}{\rho_r}\right) \times 100 \quad (\text{Eq. 2})$$

$$OP = \left(1 - \frac{\rho_e}{\rho_s}\right) \times 100 \quad (\text{Eq. 3})$$

It was then possible to deduce the open porosity inside the filaments relative to the volume of geopolymer constituting the lattices (OPF) using the following equation:

$$OPF = (OP - IFP) \times \frac{100}{100 - IFP} \quad (\text{Eq. 4})$$

Some compressive strengths are given as an indication in this study. The subject of mechanical properties related to porosity will be treated in more details in another work. The compressive strength of the samples was measured with an Instron 8562 electro-mechanical test machine (Instron, France) associated with a 5 kN load cell. The crosshead speed was set to 0.3 mm/min. The results presented are averages carried out on series of 6 samples. Results are presented as average  $\pm$  standard deviation. The upper surface of the molded geopolymers and scaffolds was cut with a low-speed saw and then lightly sanded using abrasive sheets to ensure good parallelism between the surface of the samples and the surface of the compression plates.

### 3. Results and discussion

#### 3.1. Dense geopolymers

Initially, the study was carried out on three different compositions of geopolymers without blowing agent in order to assess the impact of PEG (necessary for 3D printing) and direct ink writing on the intrinsic porosity of the geopolymers.

Table 1 summarizes all the densities and different types of porosities of the different compositions.

G 0Al M, containing no additive, has a total porosity of  $34.2 \pm 3.1\%$ ,

a result in line with those of the literature for similar compositions [20–22].

Mercury intrusion porosimetry (Fig. 2) conducted on this composition shows pore access diameters of less than 1  $\mu\text{m}$  distributed into three families. The main access diameter value is around 800 nm while the two secondary ones are 220 nm and smaller than 3 nm. This last nanoscale porous network has been reported in the literature and has been attributed to the expulsion of water trapped within the structure during the network gelation [21].

If PEG is added to the composition (GP 0Al M), the main access diameter located at 800 nm disappears. The new main access diameter is then around 40 nm, although a second and a third distribution are still present around 220 nm and 3 nm. The total porosity, and mainly the open porosity, also increased compared to G 0Al M.

In this study, PEG is used as a rheological modifier to enable 3D printing. In particular, it imparts a gel like behaviour to the paste. This behaviour may be explained by the fact that PEG is known to adsorb on the geopolymer matrix and to decrease the surface tension of water when in solution [23–25]. These phenomena may lead to stronger capillary forces by bringing the metakaolin particles closer to each, explaining a higher viscosity, which will lead to more air trapped within the paste (Fig. 3). The fact that the capillary forces are stronger may explain the decrease in pore access diameters.

Regarding the samples GP 0Al R, the mercury intrusion porosimetry curves are very similar to the previous composition. However, the distribution of the access diameters of the pores now only has two values, with a main one located at 28 nm and the secondary one still smaller than 3 nm. The extrusion process through the 840  $\mu\text{m}$  needle appears to close or reduce the pore access diameters larger than 100 nm.

Moreover, according to Table 1, the porosity of these samples is mainly due to the spacing between the filaments, but the porosity intrinsic to the geopolymer (OPF), although it is subject to a high uncertainty, remains lower than the open porosity of GP 0Al M (OP). This suggests that the process tends to densify the geopolymer, probably by releasing the air previously trapped in the paste.

#### 3.2. Cast geopolymer foams

##### 3.2.1. Influence of organic additives

In this part, a constant quantity of aluminum powder was introduced into the geopolymers. Depending on the presence/absence and the nature of organic additives, five foams with different structures, presented in Fig. 4, were obtained. All densities and different types of porosities of the samples are grouped in Table 2.

G 0.5Al M (Fig. 4 a) presents two distinct zones. The lower part of the sample, below the red line, concentrates almost all of the material, containing very large pores. The upper part, above the line, contains almost nothing but the void, apart from the material that has remained attached to the walls of the mold. This structure can be explained by the high fluidity of the paste, which promotes coalescence, Ostwald ripening and drainage phenomena, the three being linked to each other and difficult to decorelate without *in situ* monitoring.

The addition of PEG (Fig. 4 b), whose primary function was to enable 3D printing by modifying the rheological properties, turns out to be a good way to reduce the difference between the lower and upper part of the sample and to stabilize the foam. Pores seem well interconnected and of various diameters. The near dense area (circle in red) is probably

**Table 1**  
Density and porosity of different geopolymer compositions.

Designation	True density ( $\text{g}\cdot\text{cm}^{-3}$ ) $\pm$ SD	Skeletal density ( $\text{g}\cdot\text{cm}^{-3}$ ) $\pm$ SD	Envelop density ( $\text{g}\cdot\text{cm}^{-3}$ ) $\pm$ SD	TP (vol%)	OP (vol%)	IFP (vol%)	OPF (vol% of filament)
G 0Al M	$2.18 \pm 0.09$	$2.09 \pm 0.04$	$1.43 \pm 0.01$	$34.2 \pm 3.1$	$31.5 \pm 1.7$	Not applicable	Not applicable
GP 0Al M	$2.21 \pm 0.04$	$2.09 \pm 0.01$	$1.34 \pm 0.01$	$39.3 \pm 1.5$	$35.9 \pm 0.8$	Not applicable	Not applicable
GP 0Al R	$2.21 \pm 0.04$	$2.09 \pm 0.08$	$1.08 \pm 0.04$	$51.1 \pm 2.7$	$48.2 \pm 3.9$	$28.8 \pm 2.0$	$27.0 \pm 7.5$



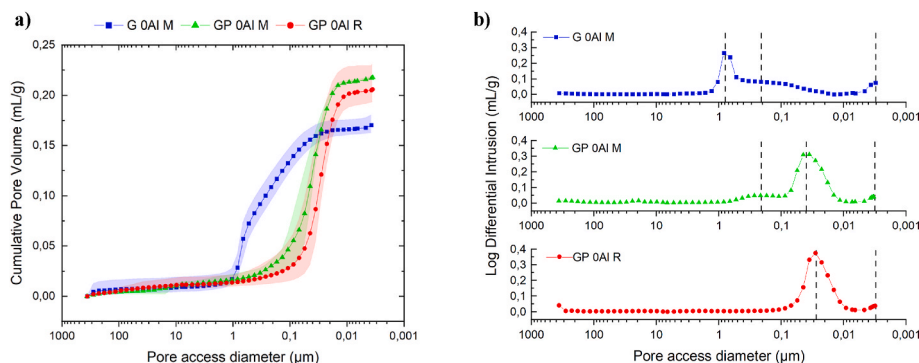


Fig. 2. (a) Cumulative intrusion of mercury inside geopolymers; (b) Log-differential intrusion curves for the different geopolymers composition.

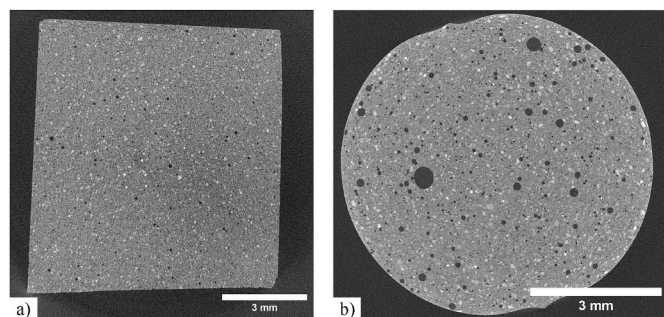


Fig. 3. X-ray tomography of a) G 0Al M and b) GP 0Al M.

due to a poor homogeneity of the distribution of aluminum powder.

The addition of surfactant, SDS or CTAB (Fig. 4 c and d), also improves the foam stability although CTAB seems to be more efficient. Both increase the viscosity of the paste, although less than PEG, thus not enough to enable direct ink writing. Pores are much more spherical than for GP 0.5Al M but seem less connected, especially in the case of CTAB. However, the latter leads to a homogeneous foam but with a compressive strength of  $0.21 \pm 0.05$  MPa. This foam is fragile and can be more easily damaged. According to Table 2, the use of surfactant alone leads to higher total porosity than in the other compositions. This could be explained by the fact that these ionic surfactants are placed at the gas-geopolymer interface, reducing the surface tension. The surfactant layers on both sides of the water film separating two bubbles repel each other due to electrostatic interactions [26]. The structure is then less subject to coalescence phenomena, the pores are more spherical and closed and the gas is probably better retained.

These improvements in stability with the addition of organic additives are also probably due to the significant increase in viscosity, especially for composition containing PEG or CTAB. Indeed, several studies in the literature show that this higher viscosity leads to the attenuation or even the suppression of drainage and ripening phenomena and better foam stabilization [27,28]. The viscosity of the paste containing SDS is lower, resulting in a faster coalescence and/or ripening phenomena [29].

The combination of PEG and CTAB (GPC 0.5Al M, Fig. 4 e) leads to smaller and more homogeneous pores than in GP 0.5Al M. Besides, pores

seem to be more interconnected and less spherical than in GC 0.5Al M. The samples have a compressive strength of  $2.4 \pm 0.8$  MPa which make them less fragile and easier to handle.

As a result, although the combination of the two organic additives leads to a lower total porosity, the composition containing both PEG and CTAB seems a good compromise between porosity, homogeneity, connectivity and mechanical resistance of the foam. This combination of additives will be used for the remaining of the study.

### 3.2.2. Influence of aluminum powder concentration on geopolymer containing PEG and CTAB

The Fig. 5 shows photographs of cut geopolymer foams containing varying amounts of aluminum powder for a fixed amount of CTAB and PEG. Table 3 groups all densities and different types of porosities of the samples. The results of the composition without aluminum powder (studied in 3.1) are shown in the table as a reference.

By multiplying the amount of aluminum powder by 10, going from 0.1 to 1 wt% of powder, more larger pores are observed in Fig. 5.

The mercury intrusion porosimetry results presented in Fig. 6 a) and the results show in Table 3 indicate a larger and larger amount of open porosity as the aluminum amount increases, except for the foam GPC 1Al M whose results are very close to the foam GPC 0.5Al M. This suggests that the porosity has reached a plateau and will not increase further at these given PEG and CTAB concentrations.

Unlike the compositions studied in part 3.1, the pore access diameters are widely dispersed (Fig. 6 b). Indeed, the curves show a significant portion of access diameters greater than 1 μm, a portion which increases with the concentration of aluminum powder and which was not present previously. This new family of pore access diameters could

Table 2

Density and porosity of different geopolymers composition containing organic additives and fixed amount of aluminum powder.

Designation	True density (g.cm <sup>-3</sup> ) ± SD	Envelop density (g.cm <sup>-3</sup> ) ± SD	TP (vol%)
G 0.5Al M	2.17 ± 0.01	0.31 ± 0.03	85.8 ± 1.5
GP 0.5Al M	2.12 ± 0.03	0.43 ± 0.03	79.7 ± 1.7
GS 0.5Al M	2.20 ± 0.01	0.28 ± 0.01	87.3 ± 0.5
GC 0.5Al M	2.16 ± 0.05	0.28 ± 0.02	87.0 ± 1.2
GPC 0.5Al M	2.18 ± 0.06	0.65 ± 0.05	70.1 ± 3.1

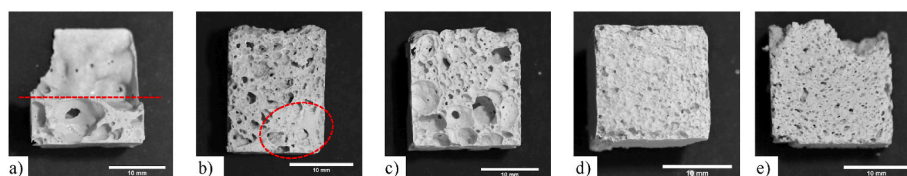


Fig. 4. Digital photographs of (a) G 0.5Al M (b) GP 0.5Al M (c) GS 0.5Al M (d) GC 0.5Al M (e) GPC 0.5Al M.

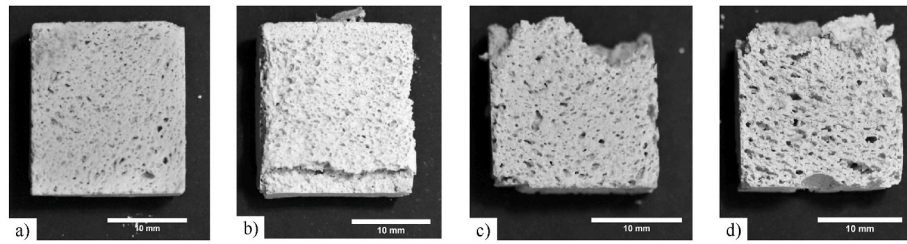


Fig. 5. Digital photographs of (a) GPC 0.1Al M (b) GPC 0.2Al M (c) GPC 0.5Al M (d) GPC 1Al M.

Table 3

Density and porosity of different geopolymers composition containing a variable amount of aluminum powder and fixed amount of CTAB and PEG.

Designation	True density (g.cm <sup>-3</sup> ) ± SD	Skeletal density (g. cm <sup>-3</sup> ) ± SD	Envelop density (g. cm <sup>-3</sup> ) ± SD	TP (vol%)	OP (vol%)
GP 0Al M	2.21 ± 0.04	2.09 ± 0.01	1.34 ± 0.01	39.3 ± 1.5	35.9 ± 0.8
GPC 0.1Al M	2.16 ± 0.03	1.91 ± 0.09	0.90 ± 0.06	58.3 ± 3.4	54.0 ± 4.0
GPC 0.2Al M	2.18 ± 0.06	1.86 ± 0.03	0.74 ± 0.03	66.0 ± 2.3	64.7 ± 2.3
GPC 0.5Al M	2.18 ± 0.06	1.89 ± 0.15	0.65 ± 0.05	70.1 ± 3.1	65.2 ± 5.4
GPC 1Al M	2.15 ± 0.06	1.95 ± 0.08	0.61 ± 0.02	71.6 ± 1.7	68.6 ± 2.3

be attributed to dihydrogen leakage. It can be assumed that with an increase in the concentration of aluminum powder, the gas flow increases, the bubbles are more and more numerous, their proximity leads to larger diameter connections with each other, which increases the size of the exhaust channels. From 0.5 wt% Al, the size of the channels continues to increase contrary to the total porosity. It is possible that the gas flow is too high for the gas to be effectively retained inside the structure.

Below 1 μm, GPC 0.1Al M and GPC 0.2Al M present a pore access distribution which recalls that of the compositions GP 0Al M and GP 0Al R studied in part 3.1 although the main access diameter of this family is a bit lower, around 22 nm. This lower value might be explained by the presence of CTAB which can further limit the mobility of the system by being absorbed on the metakaolin particles, and/or by closing access to the pores when placed at the gas/geopolymer interfaces.

The family of pores around 22 nm seems to be less and less present and more distributed with the increase in the concentration of aluminum powder, probably because the water/gas escape is preferentially through the larger diameter channels greater than 1 μm which become more and more important. As for the geopolymer without aluminum powder, pores with access diameters smaller than 3 nm are

observed which does not seem to be impacted by organic additives or the presence of aluminum.

### 3.3. 3D printed geopolymer foams

Fig. 7 groups X-ray tomographies of lattice-printed geopolymers. These images suggest that even only 0.1 wt% of aluminum powder is enough to introduce more porosity within the filaments. The change from 0.1 wt% Al to 0.2 wt% Al seems to increase the porosity and in particular the pores diameters. But there does not seem to be a noticeable difference between the compositions containing 0.2, 0.5 and 1 wt% Al. These observations are consistent with the calculated internal porosity values of the filaments presented in Table 4. The addition of 0.1 wt% Al allows to increase the porosity from  $27.0 \pm 7.5\%$  to  $45.3 \pm 5.0\%$  inside the filaments. Beyond 0.2 wt% of aluminum powder, the internal porosity of the filaments no longer increases, and since the porosity between the filaments is almost constant for the compositions containing aluminum powder, the total porosity does not vary. At the same time, the compressive strength of these samples varies very little and is around 3 MPa. Compressive strength of GPC 0.5Al R is  $3.2 \pm 0.6$  MPa, which is superior to GPC 0.5Al M compositions. This result is consistent with the fact that the total porosity of this composition is lower than the total porosity of GPC 0.5Al M.

These results are rather close to existing literature, although this comparison is made difficult by the fact that the porosity of geopolymers varies depending on their composition and drying conditions. The results can extend over very wide ranges of compressive strength. G. Franchin et al. [15] printed lattices with a similar composition presenting a compressive strength of  $2.0 \pm 0.5$  MPa for a total porosity of  $71.27 \pm 0.75$  vol%. N.P.F Gonçalves et al. [17] produced lattices with a compressive strength of  $17.31 \pm 1.13$  MPa for 65.88% total porosity. It should also be noted that in these works, the porosity was created by playing on the spacing between the filaments while in our case, a

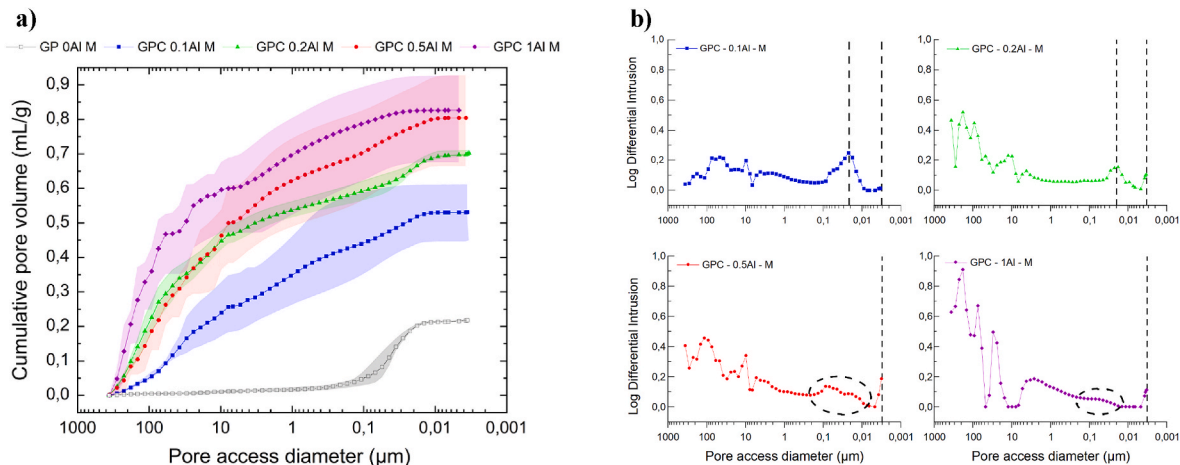
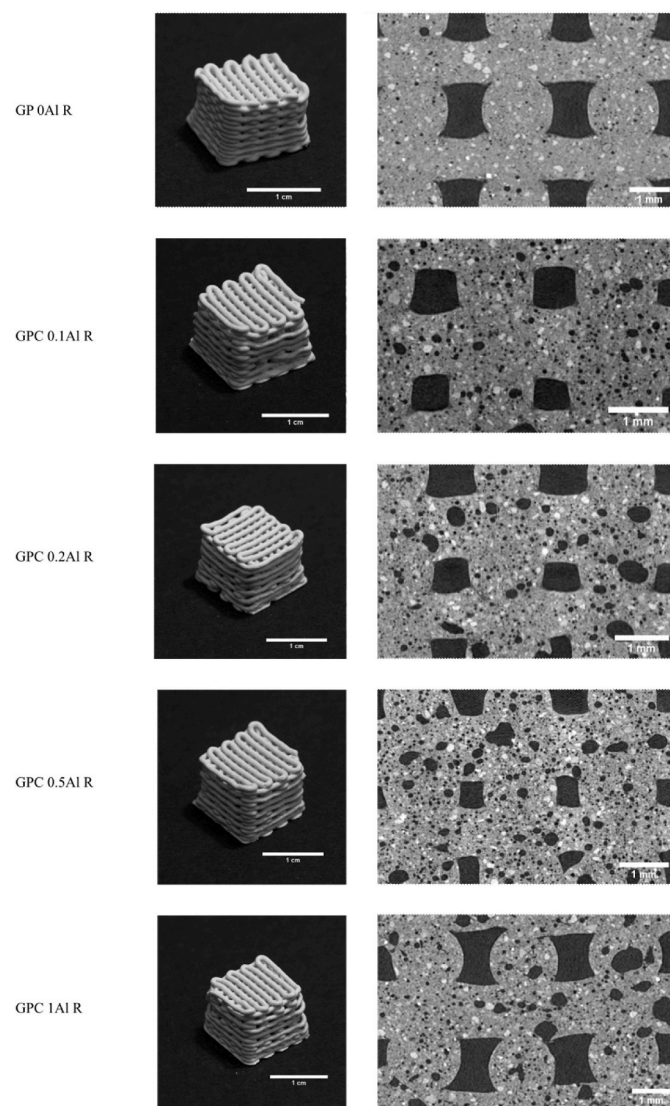


Fig. 6. (a) Cumulative intrusion of mercury and (b) log-differential intrusion curves for different geopolymers composition containing a variable amount of aluminum powder and fixed amount of CTAB and PEG.



**Fig. 7.** Digital photographs and X-ray tomographies of (a) GP 0Al R (b) GPC 0.1Al R (c) GPC 0.2Al R (d) GPC 0.5Al R (e) GPC 1Al R.

significant part of the porosity is located inside the filament itself. By adding porous fillers in the geopolymer paste, K.G. Oliveira et al. [30] printed lattices with a compressive strength of  $5.2 \pm 0.8$  MPa for a total porosity of  $67.2 \pm 0.2\%$ .

The porosity between the filaments drops when aluminum powder is added to the paste. This is due to the fact the porous filaments tend to be a bit larger and sag more than filaments without blowing agent. Fidelity to the 3D model is therefore less precise when adding aluminum powder as shown in Fig. 7. The lattices exhibit a more pronounced slump when aluminum powder is introduced into the paste, probably because of filament's discontinuities due to air evacuation during printing.

As already observed in section 3.1, the open porosity inside the geopolymer itself is lower when it is subjected to 3D printing rather than molding. Indeed, a slight porosity decrease of about 20% (the ratios of open porosity of the filaments divided by the open porosity of the corresponding foams are about 0.8), is measured for all the extruded materials which confirms that the 3D printing by extrusion tends to densify the foam while preserving about 80% of the porosity.

Besides, the porosimetry curves in Fig. 8 show that the porosity with an access diameter greater than  $1 \mu\text{m}$  has been greatly reduced, in particular for low powder concentrations (0.1 and 0.2 wt%), compared to molded foams with identical compositions. The peak observed at  $24 \mu\text{m}$  for the GPC 0.2Al R sample is not reproducible and probably comes from an anomaly. The 3D printing process tends to close the channels created for dihydrogen escape, maybe under the effect of the pressure applied to extrude the paste. The high shear rate close to nozzle wall may also create a denser skin around the filament, attributing the volume of large internal pores to small access diameters.

Pore access diameters below  $1 \mu\text{m}$  are still present, suggesting that these channels have either resisted the printing process or developed after printing. All the curves have a peak for the access diameter below  $3 \text{ nm}$ , confirming that these small accesses are not impacted by the printing process or the composition of the geopolymer. This is consistent with the hypothesis of water expulsion during the gelation, phenomenon that continues after printing, and also water evacuation during curing, thus leaving a small network.

#### 4. Conclusion

In this study, direct ink writing and chemical foaming were successfully combined to create geopolymer lattices porous at different scales. Chemical foaming, realized by aluminum powder addition, adds a statistic porosity inside the filaments while direct ink writing allows to more precisely control the macroscopic porosity and the design of the final parts. The lattices obtained by 3D printing have an open porosity of the order of 65% from 0.2 wt% aluminum powder which is similar to the molded lightweight geopolymers with same compositions. However, pore access diameters are very different depending on the shaping technique. Indeed, in molded lightweight geopolymers, the evacuation of dihydrogen creates large channels with access diameters greater than  $1 \mu\text{m}$  whose presence increases with the increase in aluminum powder concentration. During direct ink writing, these large channels are most probably compressed and closed because of the pressure applied for the foam extrusion and of the skin created around the filaments. Besides, the process tends to evacuate the air trapped within the paste, leading to a lower intrinsic porosity inside the filaments than for molded lightweight geopolymers. Still 80% of the open porosity present before extrusion is preserved and the 20% loss is compensated by the porosity between the filaments added by 3D printing.

Whatever the shaping technique used, a network with a pore access diameter of less than  $1 \mu\text{m}$  is always present, probably linked to the expulsion of water during gelation and/or its evacuation during curing, steps that continue to take place after shaping.

Finally, PEG and CTAB were the most effective organic additives for stabilizing molded foams. Even if their combination leads to lower open porosity than if there are used separately, it represents a good

**Table 4**

Density and porosity of different geopolymer lattices containing a variable amount of aluminum powder and fixed amount of CTAB and PEG \*no CTAB was added in the absence of blowing agent.

Designation	True density ( $\text{g.cm}^{-3}$ ) $\pm$ SD	Skeletal density ( $\text{g.cm}^{-3}$ ) $\pm$ SD	Envelop density ( $\text{g.cm}^{-3}$ ) $\pm$ SD	TP (vol%)	OP (vol%)	IFP (vol%)	OPF (vol% of filament)
GP 0Al R*	$2.21 \pm 0.04$	$2.09 \pm 0.08$	$1.08 \pm 0.04$	$51.1 \pm 2.7$	$48.2 \pm 3.9$	$28.8 \pm 2.0$	$27.0 \pm 7.5$
GPC 0.1Al R	$2.16 \pm 0.03$	$1.95 \pm 0.04$	$0.83 \pm 0.04$	$61.6 \pm 2.4$	$57.4 \pm 2.9$	$21.9 \pm 1.8$	$45.3 \pm 5.0$
GPC 0.2Al R	$2.18 \pm 0.06$	$2.07 \pm 0.06$	$0.70 \pm 0.03$	$67.9 \pm 2.3$	$66.1 \pm 2.4$	$23.4 \pm 5.2$	$55.5 \pm 6.3$
GPC 0.5Al R	$2.18 \pm 0.06$	$1.99 \pm 0.03$	$0.75 \pm 0.05$	$65.6 \pm 3.3$	$62.3 \pm 3.1$	$22.9 \pm 5.4$	$50.5 \pm 7.6$
GPC 1Al R	$2.15 \pm 0.06$	$2.02 \pm 0.07$	$0.74 \pm 0.04$	$65.5 \pm 2.8$	$63.3 \pm 3.3$	$25.7 \pm 3.5$	$50.3 \pm 6.8$



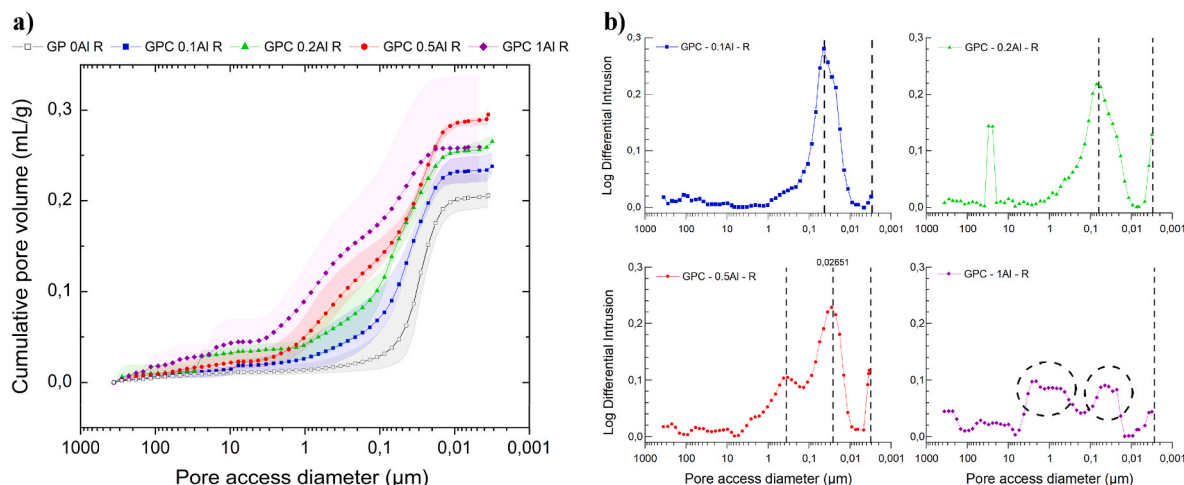


**Fig. 8.** (a) Cumulative intrusion of mercury and (b) log-differential intrusion curves for different geopolymer lattices containing a variable amount of aluminum powder and fixed amount of CTAB and PEG.

compromise between porosity, homogeneity, connectivity and resistance of the foam.

Further studies need to be performed to better understand the mechanisms that come into play during the creation of the porous network as well as those in the stabilization of geopolymer foams and their evolution during 3D printing.

These lightweight geopolymers were developed to be tested as host materials for hygroscopic salts for energy storage applications. As the materials developed in this study have the characteristics required for this type of application (multi-scale porosity greater than 65 vol% associated with compressive strengths around 3 MPa), they will be able to be associated with salts and undergo energy storage tests.

### Declaration of competing interest

The authors declare that they have no known competing financial interests or personal relationships that could have appeared to influence the work reported in this paper.

### Acknowledgements

This work was supported by the LABEX iMUST of the University of Lyon (ANR-10-LABX-0064), created within the “Plan France 2030” set up by the French government and managed by the French National Research Agency (ANR). INSA Lyon through “Enjeu Energie” and Ingé’Lyse (FR CNRS 3411) are acknowledged for their financial support.

### References

- [1] P.N. Lemounga, K. tuo Wang, Q. Tang, U.C. Melo, X. min Cui, Recent developments on inorganic polymers synthesis and applications, Elsevier Ltd, *Ceram. Int.* 42 (14) (Nov. 01, 2016) 15142–15159, <https://doi.org/10.1016/j.ceramint.2016.07.027>.
- [2] A.A. Siyal, et al., A review on geopolymers as emerging materials for the adsorption of heavy metals and dyes, Academic Press, *J. Environ. Manag.* 224 (Oct. 15, 2018) 327–339, <https://doi.org/10.1016/j.jenvman.2018.07.046>.
- [3] Y.J. Zhang, Z.C. Han, P.Y. He, H. Chen, Geopolymer-based catalysts for cost-effective environmental governance: a review based on source control and end-of-pipe treatment, Elsevier Ltd, *J. Clean. Prod.* 263 (Aug. 01, 2020), 121556, <https://doi.org/10.1016/j.jclepro.2020.121556>.
- [4] X. Ke, V.A. Baki, Assessing the suitability of alkali-activated metakaolin geopolymer for thermochemical heat storage, *Microporous Mesoporous Mater.* 325 (Oct. 2021), 111329, <https://doi.org/10.1016/j.micromeso.2021.111329>.
- [5] Y. Ettahiri, et al., A state-of-the-art review of recent advances in porous geopolymer: applications in adsorption of inorganic and organic contaminants in water, *Construct. Build. Mater.* 395 (Sep. 2023), 132269, <https://doi.org/10.1016/j.conbuildmat.2023.132269>.
- [6] P. Duxson, A. Fernández-Jiménez, J.L. Provis, G.C. Lukey, A. Palomo, J.S.J. van Deventer, Geopolymer technology: the current state of the art, *J. Mater. Sci.* 42 (9) (Nov. 2007) 2917–2933, <https://doi.org/10.1007/s10853-006-0637-z>.
- [7] C.F. Maitland, C.E. Buckley, B.H. O’Connor, P.D. Butler, R.D. Hart, Characterization of the pore structure of metakaolin-derived geopolymers by neutron scattering and electron microscopy, *J. Appl. Crystallogr.* 44 (4) (Aug. 2011) 697–707, <https://doi.org/10.1107/S0021889811021078>.
- [8] L. Tabard, E. Prud’Homme, V. Garnier, L. Gremillard, Hierarchical salt-ceramic composites for efficient thermochemical energy storage, *Appl. Mater. Today* 20 (Sep. 2020), 100658, <https://doi.org/10.1016/j.apmt.2020.100658>.
- [9] C. Bai, P. Colombo, Processing, properties and applications of highly porous geopolymers: a review, Elsevier Ltd, *Ceram. Int.* 44 (14) (Oct. 01, 2018) 16103–16118, <https://doi.org/10.1016/j.ceramint.2018.05.219>.
- [10] R.M. Novais, R.C. Pullar, J.A. Labrincha, Geopolymer foams: an overview of recent advancements, Elsevier Ltd, *Prog. Mater. Sci.* 109 (Apr. 01, 2020), 100621, <https://doi.org/10.1016/j.pmatsci.2019.100621>.
- [11] D. Kitnasamy, K. Pasupathy, S. Ramakrishnan, J. Sanjayan, Progress, current thinking and challenges in geopolymer foam concrete technology, *Cem. Concr. Compos.* 116 (Nov. 2020), 103886, <https://doi.org/10.1016/j.cemconcomp.2020.103886>.
- [12] E. Papa, et al., Synthesis of porous hierarchical geopolymer monoliths by ice-templating, *Microporous Mesoporous Mater.* 215 (Jun. 2015) 206–214, <https://doi.org/10.1016/j.micromeso.2015.05.043>.
- [13] D. Medpelli, J.-M. Seo, D.-K. Seo, Geopolymer with hierarchically meso-/macroporous structures from reactive emulsion templating, *J. Am. Ceram. Soc.* 97 (1) (Jan. 2014) 70–73, <https://doi.org/10.1111/jace.12724>.
- [14] V. Kočí, R. Černý, Directly foamed geopolymers: a review of recent studies, *Cem. Concr. Compos.* 130 (Jul. 2022), 104530, <https://doi.org/10.1016/j.cemconcomp.2022.104530>.
- [15] G. Franchin, et al., Direct ink writing of geopolymeric inks, *J. Eur. Ceram. Soc.* 37 (6) (Nov. 2017) 2481–2489, <https://doi.org/10.1016/j.jeurceramsoc.2017.01.030>.
- [16] S. Ma, et al., Direct ink writing of geopolymer with high spatial resolution and tunable mechanical properties, *Addit. Manuf.* 46 (Oct. 2021), 102202, <https://doi.org/10.1016/j.addma.2021.102202>.
- [17] N.P.F. Gonçalves, S.M. Olhero, J.A. Labrincha, R.M. Novais, 3D-printed red mud/metakaolin-based geopolymers as water pollutant sorbents of methylene blue, *J. Clean. Prod.* 383 (Jan. 2023), 135315, <https://doi.org/10.1016/j.jclepro.2022.135315>.
- [18] B. Coppola, C. Tardivat, S. Richaud, J.M. Tulliani, L. Montanaro, P. Palmero, 3D printing of dense and porous alkali-activated refractory wastes via Direct Ink Writing (DIW), *J. Eur. Ceram. Soc.* 41 (6) (Jun. 2021) 3798–3808, <https://doi.org/10.1016/j.jeurceramsoc.2021.01.019>.
- [19] S. Yan, F. Zhang, S. Wang, P. He, D. Jia, J. Yang, Crystallization behavior and mechanical properties of high open porosity dolomite hollow microspheres filled hybrid geopolymer foams, *Cem. Concr. Compos.* 104 (Nov. 2019), 103376, <https://doi.org/10.1016/j.cemconcomp.2019.103376>.
- [20] D.S. Perera, O. Uchida, E.R. Vance, K.S. Finnie, Influence of curing schedule on the integrity of geopolymers, *J. Mater. Sci.* 42 (9) (May 2007) 3099–3106, <https://doi.org/10.1007/s10853-006-0533-6>.
- [21] P. Duxson, J.L. Provis, G.C. Lukey, S.W. Mallicoate, W.M. Kriven, J.S.J. Van Deventer, Understanding the relationship between geopolymer composition, microstructure and mechanical properties, *Colloids Surfaces A Physicochem. Eng. Asp.* 269 (1–3) (Nov. 2005) 47–58, <https://doi.org/10.1016/j.colsurfa.2005.06.060>.
- [22] V. Benavent, F. Frizon, A. Poulesquen, Effect of composition and aging on the porous structure of metakaolin-based geopolymers, *J. Appl. Crystallogr.* 49 (6) (Dec. 2016) 2116–2128, <https://doi.org/10.1107/S1600576716014618>.
- [23] R. Zhang, P. Somasundaran, Advances in adsorption of surfactants and their mixtures at solid/solution interfaces, *Adv. Colloid Interface Sci.* 123–126 (Nov. 16, 2006) 213–229, <https://doi.org/10.1016/j.cis.2006.07.004>. SPEC. ISS. Elsevier.



- [24] M. Catauro, F. Papale, G. Lamanna, F. Bollino, Geopolymer/PEG hybrid materials synthesis and investigation of the polymer influence on microstructure and mechanical behavior, *Mater. Res.* 18 (4) (Jul. 2015) 698–705, <https://doi.org/10.1590/1516-1439.342814>.
- [25] M. Tönsmann, D.T. Ewald, P. Scharfer, W. Schabel, Surface tension of binary and ternary polymer solutions: experimental data of poly(vinyl acetate), poly(vinyl alcohol) and polyethylene glycol solutions and mixing rule evaluation over the entire concentration range, *Surface. Interfac.* 26 (Oct. 2021), 101352, <https://doi.org/10.1016/j.surfin.2021.101352>.
- [26] B. Feneuil, O. Pitois, N. Roussel, Effect of surfactants on the yield stress of cement paste, *Cement Concr. Res.* 100 (Oct. 2017) 32–39, <https://doi.org/10.1016/j.cemconres.2017.04.015>.
- [27] I. Lesov, S. Tcholakova, N. Denkov, Factors controlling the formation and stability of foams used as precursors of porous materials, *J. Colloid Interface Sci.* 426 (Jul. 2014) 9–21, <https://doi.org/10.1016/j.jcis.2014.03.067>.
- [28] S. Guignot, S. Faure, M. Vignes-Adler, O. Pitois, Liquid and particles retention in foamed suspensions, *Chem. Eng. Sci.* 65 (8) (Apr. 2010) 2579–2585, <https://doi.org/10.1016/j.ces.2009.12.039>.
- [29] S. Petlitckaia, A. Poulesquen, Design of lightweight metakaolin based geopolymer foamed with hydrogen peroxide, *Ceram. Int.* 45 (1) (Nov. 2019) 1322–1330, <https://doi.org/10.1016/j.ceramint.2018.10.021>.
- [30] K.G. Oliveira, et al., Geopolymer beads and 3D printed lattices containing activated carbon and hydrotalcite for anionic dye removal, *Catal. Today* 390 (391) (May 2022) 57–68, <https://doi.org/10.1016/j.cattod.2021.12.002>.